2023-12

A two-dimensional double layer-averaged model of hyperconcentrated turbidity currents with non-Newtonian rheology

Sun, Y

10.1016/j.ijsrc.2023.08.002
International Journal of Sediment Research
Elsevier BV

Supporting Information for

A 2D double layer-averaged model of hyperconcentrated turbidity currents with non-Newtonian rheology

Yining Sun[1], Ji Li[1,2], Zhixian Cao[1*] and Alistair G.L. Borthwick[3,4]

1 State Key Laboratory of Water Resources and Hydropower Engineering Science, Wuhan University, Wuhan 430072, China

2 Zienkiewicz Centre for Computational Engineering, Faculty of Science and Engineering, Swansea University, Swansea SA1 8EN, UK

3 Institute for Infrastructure and Environment, The University of Edinburgh, Edinburgh EH9 3JL, UK

4 School of Engineering, Computing and Mathematics, University of Plymouth, Plymouth PL4 8AA, UK

Correspondence

* Zhixian Cao, State Key Laboratory of Water Resources and Hydropower Engineering Science, Wuhan University, Wuhan 430072, China. E-mail: zxcao@whu.edu.cn

Contents of this file

Text S1 Mathematical model

Structure of double layer-averaged model

Fig. S1 presents the general structure of subaqueous sediment-laden flow, which comprises: (i) an upper clear-water flow layer, (ii) a lower sediment-laden flow layer (i.e., turbidity current), and (iii) an erodible bed with vanishing velocity. Interactions occur at the interfaces between the upper layer clear water flow, sediment-laden flow and erodible bed. The upper layer interacts with the lower sediment-laden flow layer by exchanging clear water, whereas the lower sediment-laden flow layer exchanges both water and sediment with the erodible bed.

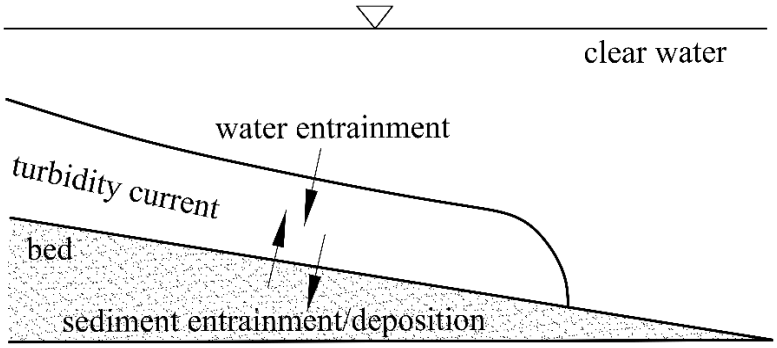

Fig. S1. Sketch of subaqueous sediment-laden flow.

Governing equations

For the lower sediment-laden flow layer, application of the mass and momentum conservation laws leads to continuity and momentum equations, which are written in Cartesian tensor notation as follows:

$$\frac{\partial \rho_c}{\partial t} + \frac{\partial (\rho_c u_{si})}{\partial x_i} = 0 \tag{S1.1}$$

$$\frac{\partial(\rho_c u_{si})}{\partial t}+\frac{\partial(\rho_c u_{si}u_{sj})}{\partial x_j}=F_i-\frac{\partial p_r}{\partial x_i}+\frac{\partial \tau_{ij}}{\partial x_j} \tag{S1.2}$$

where t is time; $x_i\ (i=1,2,3)$ are horizontal and vertical Cartesian coordinates; $\rho_c=\rho_w(1-c_s)+\rho_s c_s$ is the density of the water-sediment mixture in the sediment-laden flow layer; ρ_s is sediment density; ρ_w is water density; c_s is volumetric sediment concentration; u_{si} is the *i*-th component of sediment-laden flow velocity; p_r is pressure within the sediment-laden flow layer; τ_{ij} relates to the mixture stress tensor; and F_i is the *i*-th component of the resultant mass force.

Assuming that gravity is the only mass force, then $F_x=F_y=0$ and $F_z=-\rho_c g$. We also neglect the horizontal components of normal stress τ_{xx},τ_{yy} and shear stress τ_{xy},τ_{yx}. The 2D continuity and momentum equations (S1.1) and (S1.2) for the sediment-laden flow then become:

$$\frac{\partial \rho_c}{\partial t}+\frac{\partial \rho_c u_{sx}}{\partial x}+\frac{\partial \rho_c u_{sy}}{\partial y}=0 \tag{S1.3}$$

$$\frac{\partial \rho_c u_{sx}}{\partial t}+\frac{\partial \rho_c u_{sx}^{\,2}}{\partial x}+\frac{\partial \rho_c u_{sx}u_{sy}}{\partial y}=-\frac{\partial p_r}{\partial x}+\frac{\partial \tau_{xz}}{\partial z} \tag{S1.4a}$$

$$\frac{\partial \rho_c u_{sy}}{\partial t}+\frac{\partial \rho_c u_{sx}u_{sy}}{\partial x}+\frac{\partial \rho_c u_{sy}^{\,2}}{\partial y}=-\frac{\partial p_r}{\partial y}+\frac{\partial \tau_{yz}}{\partial z} \tag{S1.4b}$$

where $x(=x_1)$ and $y(=x_2)$ are the horizontal Cartesian coordinates; $z(=x_3)$ is the vertical Cartesian coordinate above a fixed datum; and u_{sx},u_{sy} are the horizontal velocity components.

The depth-averaged quantity $\Phi(=U_s,V_s)$ of a two-dimensional variable $\phi(=u_{sx},u_{sy})$ is defined by

$$\Phi = \frac{1}{h_s}\int_{z_b}^{\eta_s} \phi dh \tag{S1.5}$$

where h_s is the thickness of the lower sediment-laden flow layer; z_b is the bed elevation; and $\eta_s = h_s + z_b$ is the elevation of the interface between the clear-water layer and sediment-laden flow layer.

Before deriving the depth-integrated model, it is necessary to introduce boundary conditions at the interface and channel bed. Noting that the channel bed usually varies at a much lower rate than the flow, the following non-slip condition is applied at the bed boundary:

$$u_{sx}\big|_{z=z_b} = 0, \quad u_{sy}\big|_{z=z_b} = 0 \tag{S1.6}$$

The interface between the lower sediment-laden flow layer and the upper clear-water flow layer is a moving boundary, and so

$$u_{sz}\big|_{z=\eta_s} = \frac{d\eta_s}{dt} + E_w = \frac{\partial \eta_s}{\partial t} + \frac{\partial \eta_s}{\partial x} u_{sx}\big|_{z=\eta_s} + \frac{\partial \eta_s}{\partial y} u_{sy}\big|_{z=\eta_s} + E_w \tag{S1.7}$$

where E_w is the velocity of water entrainment across the interface between the two layers.

Integrating the continuity equation (S.1.3) according to (S1.5) and substituting in the boundary conditions (S1.6) and (S1.7) leads to the following depth-integrated 2D continuity equation for the sediment-laden flow layer:

$$\frac{\partial \rho_c h_s}{\partial t} + \frac{\partial \rho_c h_s U_s}{\partial x} + \frac{\partial \rho_c h_s V_s}{\partial y} = \rho_w E_w - \rho_0 \frac{\partial z_b}{\partial t} \tag{S1.8}$$

where U_s and V_s are the sediment-laden flow layer-averaged velocity components in the *x*-

and y-directions; p is the bed sediment porosity; and $\rho_0 = \rho_w p + \rho_s(1-p)$ is the density of the saturated bed.

Inertial and diffusion effects in the vertical momentum equations are neglected, and hence the flow pressure p_r is assumed hydrostatic such that,

$$p_r = \rho_w g h_w + \int_{z_b}^{\eta_s} \rho_c g h dh \tag{S1.9}$$

where h_w is the thickness of upper clear-water flow layer.

Integrating the x-momentum equation (S1.4a) over the flow depth and then applying the Leibniz integral rule to this equation yields

$$\begin{aligned}
&\frac{\partial}{\partial t}\int_{z_b}^{\eta_s}(\rho_c u_{sx})dz + \frac{\partial \eta_s}{\partial t}(\rho_c u_{sx})\Big|_{z=\eta_s} - \frac{\partial z_b}{\partial t}(\rho_c u_{sx})\Big|_{z=z_b} + \frac{\partial}{\partial x}\int_{z_b}^{\eta_s}\left(\rho_c u_{sx}{}^2\right)dz + \frac{\partial \eta_s}{\partial x}\left(\rho_c u_{sx}{}^2\right)\Big|_{z=\eta_s} \\
&- \frac{\partial z_b}{\partial x}(\rho_c u_{sx})\Big|_{z=z_b} + \frac{\partial}{\partial y}\int_{z_b}^{\eta_s}(\rho_c u_{sx}u_{sy})dz + \frac{\partial \eta_s}{\partial y}(\rho_c u_{sx}u_{sy})\Big|_{z=\eta_s} - \frac{\partial z_b}{\partial y}(\rho_c u_{sx}u_{sy})\Big|_{z=z_b} \\
&= \tau_{xz}\big|_{z=\eta_s} - \tau_{xz}\big|_{z=z_b} - \left[\frac{\partial}{\partial x}\int_{\eta_s}^{\eta}(\rho_w g z)dz - \frac{\partial \eta}{\partial x}p_r\big|_{z=\eta} + \frac{\partial \eta_s}{\partial x}p_r\big|_{z=\eta_s}\right]
\end{aligned} \tag{S1.10}$$

Substituting (S1.6), (S1.7) and (S1.9) into Eq. (S1.10) yields the following depth-integrated x-momentum equation for the sediment-laden flow layer:

$$\begin{aligned}
&\frac{\partial \rho_c h_s U_s}{\partial t} + \frac{\partial}{\partial x}\left[\rho_c h_s U_s^2 + 0.5\rho_c g h_s{}^2\right] + \frac{\partial}{\partial y}(\rho_c h_s U_s V_s) = -\rho_c g h_s \frac{\partial z_b}{\partial x} + \rho_w g h_w \frac{\partial h_s}{\partial x} \\
&- \frac{\partial}{\partial x}(\rho_w g h_w h_s) + \tau_{wx} + \tau_{effx} + \rho_w E_w U_w
\end{aligned} \tag{S1.11a}$$

Similarly, integrating Eq. (S1.4b) over the flow depth leads to the following depth-integrated y-momentum equation for the sediment-laden flow layer:

$$\frac{\partial \rho_c h_s V_s}{\partial t}+\frac{\partial}{\partial y}\left[\rho_c h_s V_s^2+0.5\rho_c g h_s{}^2\right]+\frac{\partial}{\partial x}\left(\rho_c h_s U_s V_s\right)=-\rho_c g h_s\frac{\partial z_b}{\partial y}+\rho_w g h_w\frac{\partial h_s}{\partial y}$$
$$-\frac{\partial}{\partial y}(\rho_w g h_w h_s)+\tau_{wy}+\tau_{effy}+\rho_w E_w V_w \tag{S1.11b}$$

where U_w and V_w are the clear-water flow layer-averaged velocity components in the *x*- and *y*-directions; τ_{wx},τ_{wy} are shear stresses at the interface between the clear-water flow layer and the sediment-laden flow layer; $\tau_{eff}=-\left(\beta_B\tau_B+\beta_N\tau_N\right)$ is the effective shear stress, in which τ_B is the shear stress due to non-Newtonian rheology, τ_N is the shear stress due to Newtonian rheology, and β_B and β_N help control the Newtonian or non-Newtonian behavior as the sediment concentration varies.

Text S2 Model validation- subaerial mud flow

A series of experiments were conducted at the University of California by V. G. Wright and R. B. Krone to investigate mud and debris flow rheological properties (Wright, 1987; and Wright and Krone, 1987). The present EDL model is tested against one of the experiments (Run 15) involving relatively high sediment concentration, in which the subaerial mud flow acts as a non-Newtonian fluid. The experiments were conducted in a rectangular glass flume, 7.3 m long and 0.6 m wide, with a bottom slope of 0.06. A reservoir of length 1.8 m was located upstream of the flume, and a vertical sliding gate placed at the downstream end of the reservoir, as shown in Fig. S1.

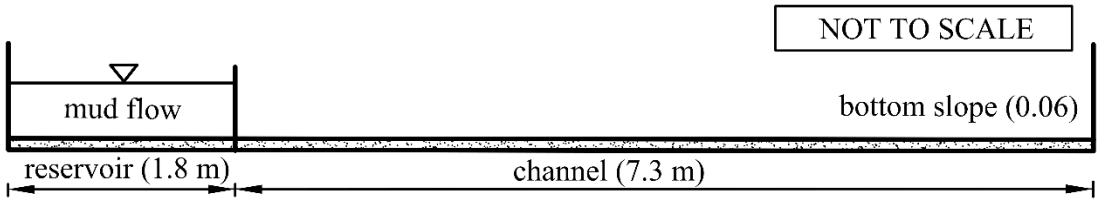

Fig. S2. Experimental setup for subaerial mud flow tests undertaken by Wright (1987) and Wright and Krone (1987).

Initial conditions of the subaerial mud flow are: height $h_{s0} = 0.3\,\mathrm{m}$; length $L = 1.8\,\mathrm{m}$; and density ρ_{c0}=1073 $\mathrm{kg/m^3}$. Wright (1987) and Wright and Krone (1987) used the following empirical expresstions to approximate the observed rheological behaviour, in terms of yield stress,

$$\tau_Y = \begin{cases} 37.991 & \gamma \le 1 \\ 23.165 - 3.966\ln(\gamma) & \gamma > 1 \end{cases}, \tag{S2.1}$$

and viscous stress,

$$\tau_V = \begin{cases} 32.2963 & \gamma \le 1 \\ 27.2458(\gamma)^{0.16} & \gamma > 1 \end{cases}, \tag{S2.2}$$

where γ denotes shear rate. The suspended material comprised bentonite with specific gravity of 2.65 and mean particle diameter of 44 μm. In the numerical model, the grid size is set to 0.02 m in both longitudinal and lateral directions.

To test the performance of our EDL model, we first compare the model predictions against an analytical solution for non-Newtonian fluid proposed by Huang and Garcia (1997), alternative numerical predictions by Imran et al. (Imran and Parker et al., 2001), and computational results using the previous ODL model (Cao and Li et al., 2015). In the ODL model, the bed roughness Manning coefficient n_b is set to $0.03\,\mathrm{m}^{-1/3}\mathrm{s}$ in order to provide a best fit to the experimental data. Fig. S3 shows that the Newtonian ODL model simulates a much longer runout than the three non-Newtonian models. This is to be expected because when non-Newtonian rheology is neglected, the boundary shear stress is not estimated properly, and so the subaerial flow thickness is incorrectly estimated. Compared against the experimental data, the three non-Newtonian models perform relatively better than the Newtonian model in estimating runout distance and thickness of the mud flow at $t = 4.1\,\mathrm{s}$ (Fig. S3). However, pronounced differences are evident in the profiles predicted by the three non-Newtonian models, with the best agreement between measured and predicted results obtained using the EDL model (where the coefficient of determination is $\mathrm{R}^2_{\mathrm{EDL}} = 0.8159$).

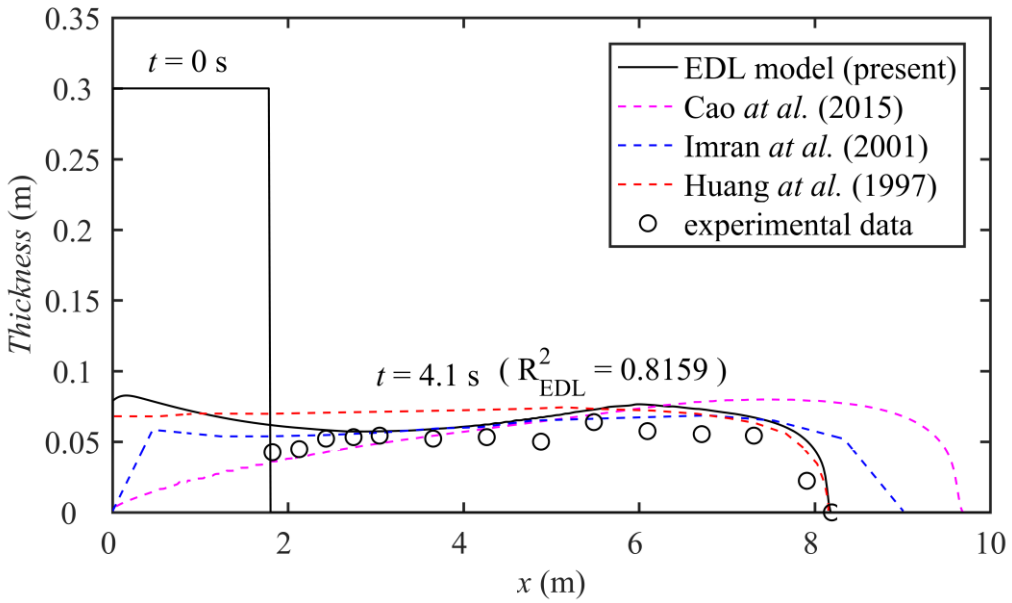

Fig. S3. Comparison between experimental and numerical thickness h_s profiles of subaerial mud flow in a rectangular channel. Experimental data from Wright (1987) and Wright and Krone (1987).

Figures S4-S6

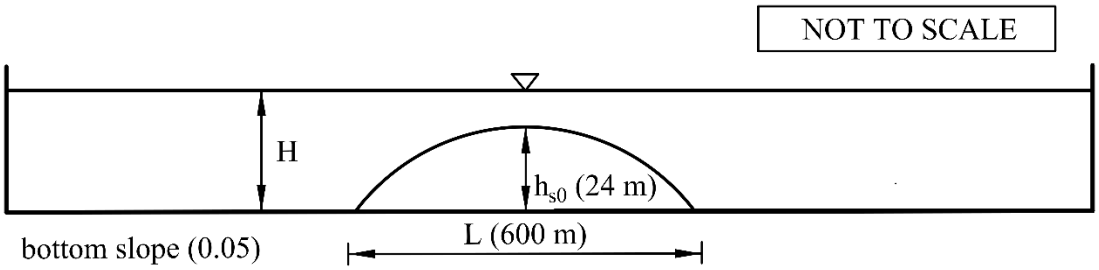

Fig. S4. Numerical domain and initial condition for subaqueous debris flow originally considered by Imran et al. (2001), where H denotes initial water depth, L is initial length of debris flow, h_{s0} is maximum initial thickness of debris flow.

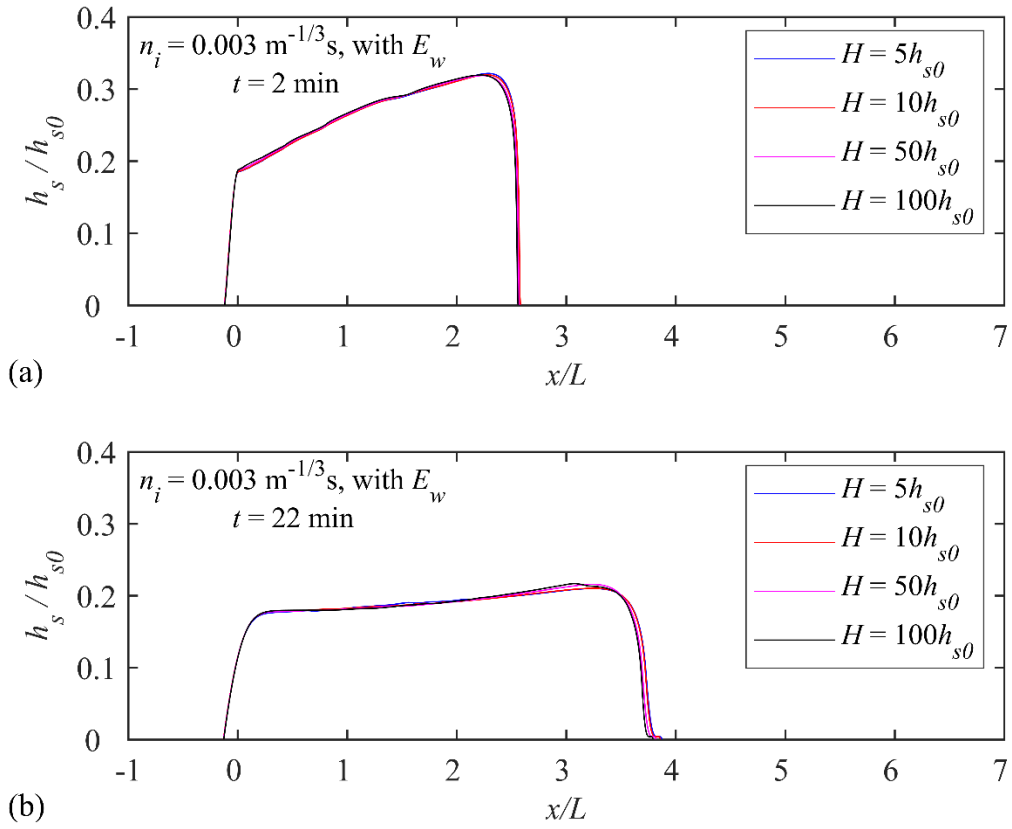

Fig. S5. Subaqueous debris flow profiles predicted by EDL model for different initial water depths H at times: (a) $t = 2\,\text{min}$; and (b) $t = 22\,\text{min}$.

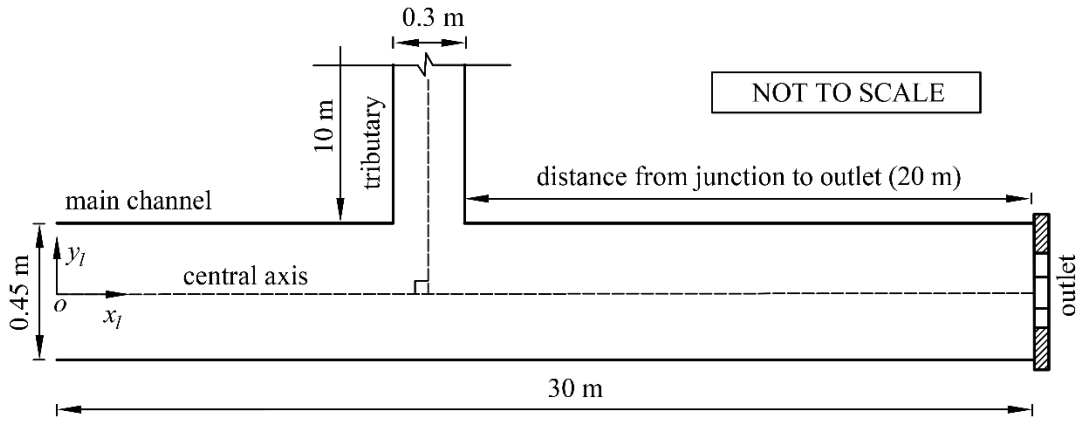

Fig. S6. Plan geometry of reservoir turbidity current experiments by Wang et al. (2020).

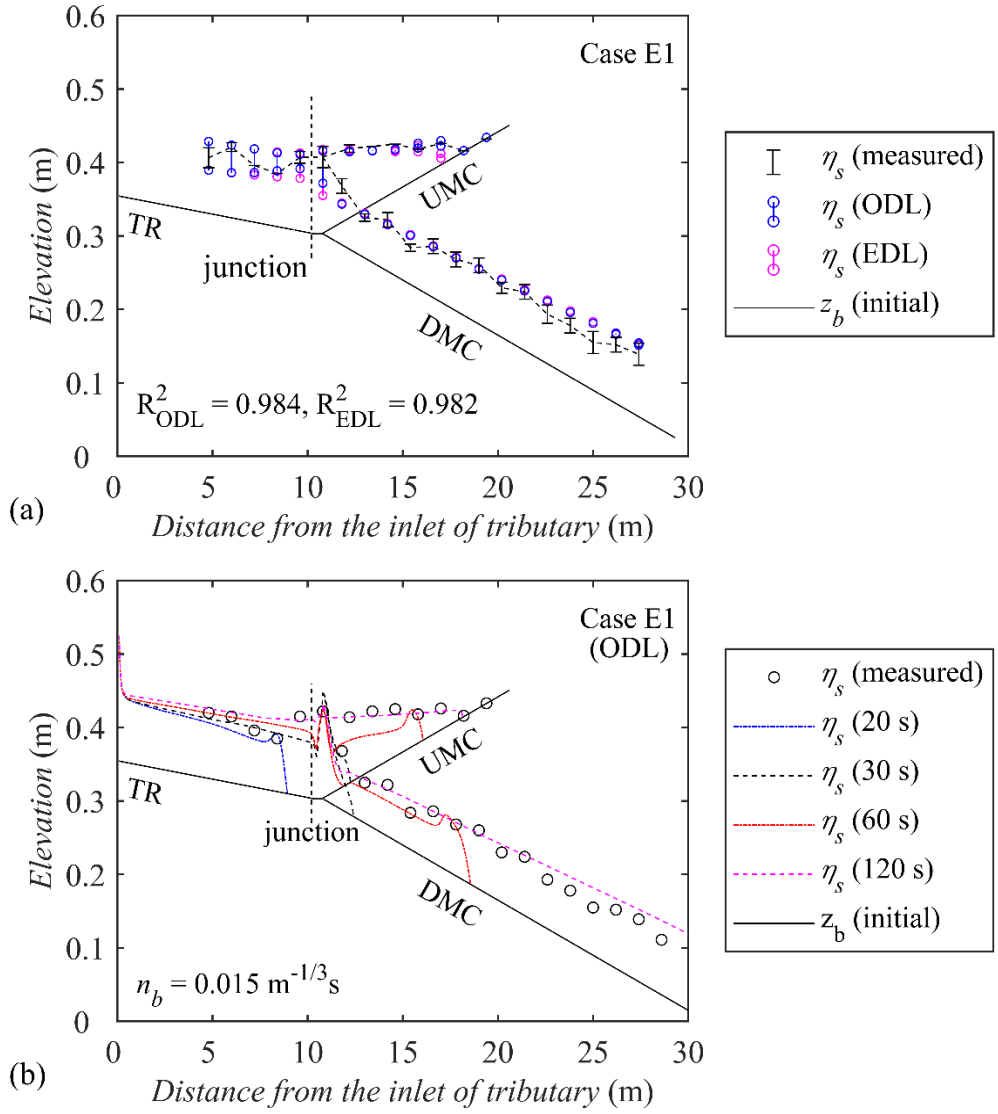

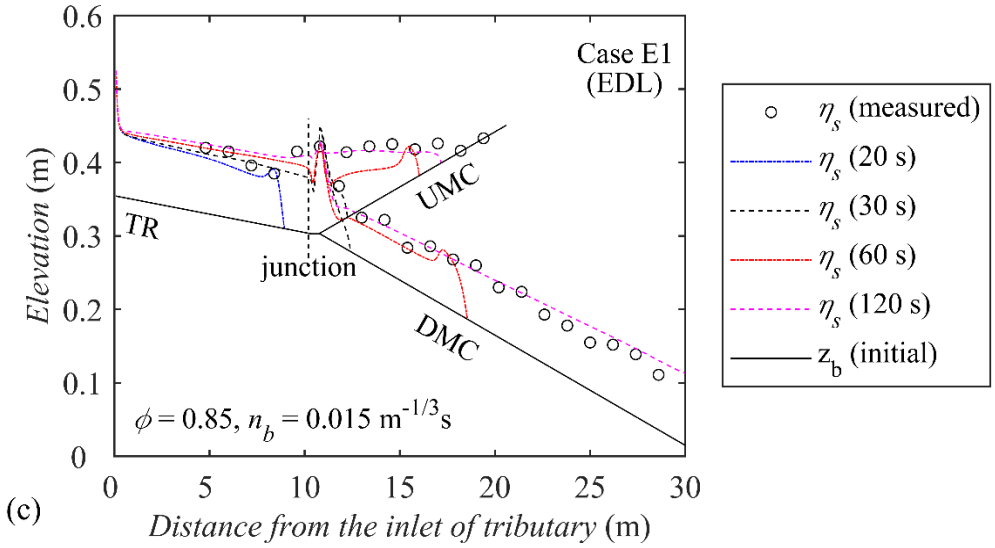

Fig. S7 Case E1 with tributary discharge $Q_t = 1.98$ L/s. (a) Comparison between measured and computed ranges of interface elevation η_s at each cross-section. (b) ODL model and (c) EDL model predictions, and experimental measurements (Wang et al., 2020) of front elevation and interface elevation profiles along the central axes of the main channel (MC) and tributary (TR) at four time instants. Abbreviations UMC and DMC refer to upstream and downstream reaches of the main channel.

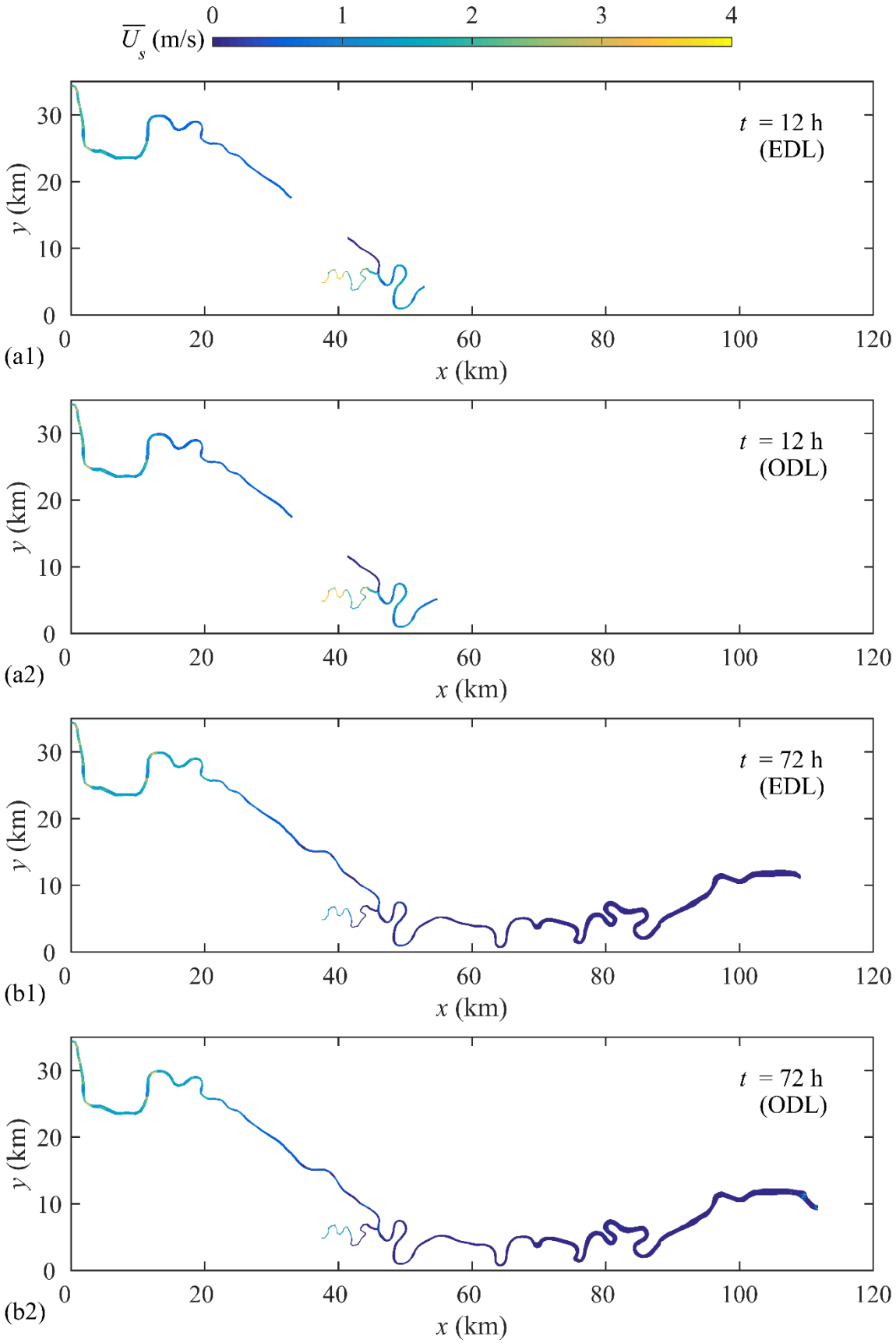

Fig. S8. Guxian reservoir study: velocity of turbidity currents at times t = 12 h and 72 h, predicted using (a1, b1) EDL model and (a2, b2) ODL model.

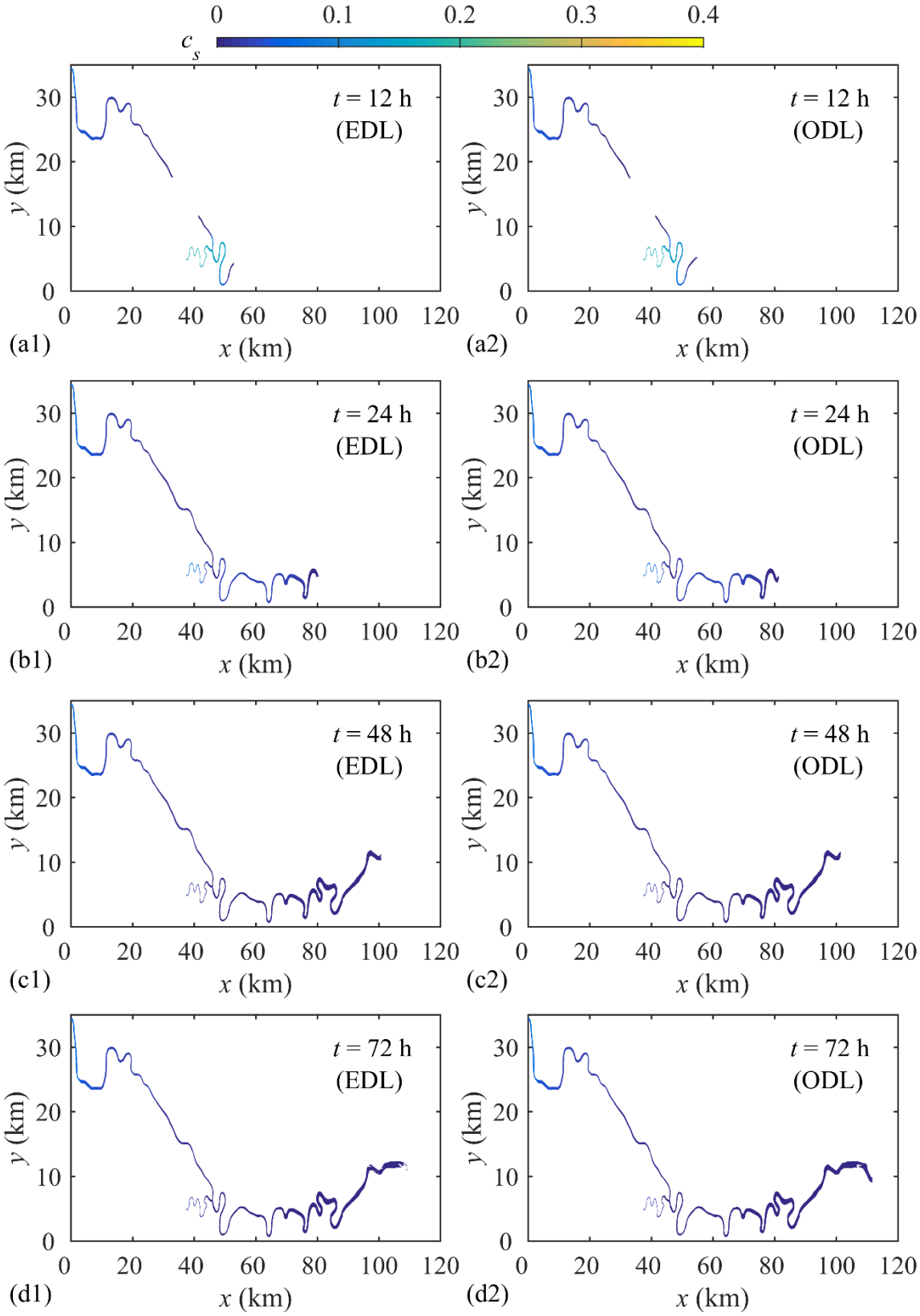

Fig. S9. Guxian reservoir model: distributions of volumetric sediment concentration c_s at times t = 12 h, 24 h, 48 h, and 72 h computed using (a1-d1) EDL model and (a2-d2) ODL model.